Applied Catalysis B: Environmental 125 (2012) 144–148

Contents lists available at SciVerse ScienceDirect

Applied Catalysis B: Environmental

journal homepage: www.elsevier.com/locate/apcatb

# $Bi_2WO_6/SiO_2$ photonic crystal film with high photocatalytic activity under visible light irradiation

Songmei Sun, Wenzhong Wang*, Ling Zhang, Jiehui Xu

*State Key Laboratory of High Performance Ceramics and Superfine Microstructure, Shanghai Institute of Ceramics, Chinese Academy of Sciences, 1295 Dingxi Road, Shanghai 200050, PR China*

ARTICLE INFO

*Article history:*
Received 2 March 2012
Received in revised form 25 May 2012
Accepted 27 May 2012

*Keywords:*
Photocatalyst
$Bi_2WO_6$ film
Phenol degradation
Photonic crystal

ABSTRACT

Immobilized $Bi_2WO_6$ thin films were successfully synthesized by direct chemical deposition on $SiO_2$ photonic crystals. The as-prepared $Bi_2WO_6/SiO_2$ photonic crystal films exhibited excellent photocatalytic decomposition of RhB and phenol under visible light irradiation. Almost 99% of the RhB molecules were degraded within 60 min and 64% of the phenol molecules were degraded within 2 h along with the sharp decrease of total organic carbon (TOC) under visible light irradiation. Comparative studies indicated that the photocatalytic activity of the $Bi_2WO_6/SiO_2$ films is about 3 times higher than that of ordinary $Bi_2WO_6$ films under the same conditions. The transmission spectrum of the $Bi_2WO_6/SiO_2$ photonic crystal films exhibited an apparent transmission dip around 550 nm originated from its photonic crystal structure. The different photocatalytic performance between the ordinary $Bi_2WO_6$ film and the $Bi_2WO_6/SiO_2$ photonic crystal film may be ascribed to their different film structures.



## 1. Introduction

Photocatalytic oxidation technique has been proven to be efficient for purifying a great variety of pollutants from water [1–6]. However, the practical photocatalytic water purification system has not yet been successfully achieved for several reasons. For example, most previous studied photocatalysts, which are in powder form, are difficult to separate from the reaction suspensions, especially when dealing with ultrafine or nanoscale catalyst particles. Furthermore, the photocatalyst residue in the reaction system may contaminate the treated water. Compared with particulate photocatalysts, immobilized photocatalysts have clear advantages, such as catalyst recovery and reuse. But they usually exhibit poor performance due to the much smaller light irradiated surface area than that of particulate photocatalysts. So improving the photocatalytic activity of immobilized photocatalysts is of great interest for the practical application of photocatalysis.

Among various studied photocatalysts, visible light driven $Bi_2WO_6$ photocatalyst is one of the most promising materials for its high stability, non-toxicity, wide solar energy response, and high photocatalytic activity [7–19]. $Bi_2WO_6$ photocatalyst has been investigated extensively for its photocatalytic degradation of organic pollutants [7–18] and the photocatalytic evolution of $O_2$ from water [19]. Nevertheless, compared with the numerous studies of particulate photocatalyst, only a few of studies focused on the immobilized $Bi_2WO_6$ photocatalyst up to the present [20–25]. Recently, $Bi_2WO_6$ inverse opals, which were prepared by a dip-coating infiltration method, were used as efficient visible-light-active photocatalysts [26]. In this paper, we propose to immobilize $Bi_2WO_6$ nanoparticles on the $SiO_2$ photonic crystal to produce much efficient photocatalysts. As is well known, $SiO_2$ photonic crystal could produce slow photons at energies slightly higher and lower than its photonic band-gap [27]. If the energy of the slow photons is in the range of the absorbance of the deposited photocatalyst or contaminant, then an enhancement of the light utilization and photocatalytic activity can be realized.

Traditional $Bi_2WO_6$ films were usually prepared by dip-coating or spin-coating method [20–24]. In the present paper, $Bi_2WO_6$ films in nanoscale were aimed to grow uniformly on a $SiO_2$ photonic crystal film substrate by a direct chemical deposition method. Because the slow photons in photonic crystal could increase the light utilization efficiency, the as-prepared $Bi_2WO_6/SiO_2$ photonic crystal film was expected to exhibit higher photocatalytic activity than that of the ordinary $Bi_2WO_6$ film. RhB and phenol were used to evaluate the photocatalytic performance of the $Bi_2WO_6$ films, which were widely used but slowly degradable in the environment. The successful realization of immobilized $Bi_2WO_6/SiO_2$ photonic crystal film with high photocatalytic activity may inspire the studies of other highly active immobilized photocatalysts.

* Corresponding author. Fax: +86 21 5241 3122.
*E-mail address:* wzwang@mail.sic.ac.cn (W. Wang).

0926-3373/$ – see front matter © 2012 Elsevier B.V. All rights reserved.
http://dx.doi.org/10.1016/j.apcatb.2012.05.039

## 2. Experimental

### 2.1. Sample preparation

#### 2.1.1. Synthesis of $SiO_2$ photonic crystal

Firstly, monodisperse $SiO_2$ spheres with about 240 nm in size were prepared using the Stöber method from the sol-gel process of tetraethyl orthosilicate (TEOS) under base catalysis. Briefly, 15 mL of TEOS were dissolved in 100 mL of absolute ethanol, and 25 mL of 25% aqueous ammonia were dissolved in 150 mL of absolute ethanol. These two solutions were mixed together and stirred for 3 h at 40 °C. The resultant $SiO_2$ spheres were isolated and washed. The $SiO_2$ photonic crystal template was prepared by an established vertical-deposition technique. A glass slide was held vertically in a 6 mL vial containing an ethanol suspension of the obtained monodisperse $SiO_2$ spheres (0.6%). As the ethanol evaporated and the meniscus swept down the substrate, capillary forces induced ordering of the spheres on both sides of the glass slide. Then the $SiO_2$ photonic crystal substrate was obtained. The as-prepared $SiO_2$ photonic crystal substrate was sintered at 400 °C for 1 h before used.

#### 2.1.2. Synthesis of $Bi_2WO_6/SiO_2$ photonic crystal films

Typically, 0.8 mmol of $Bi(NO_3)_3{\cdot}5H_2O$ was dissolved in 30 mL of 2-methoxyethanol. 0.4 mmol of $Na_2WO_4$ was dissolved in 10 mL of ethylene glycol. These two solutions were mixed together in 100 mL flask and was added a 2 cm × 2 cm $SiO_2$ photonic crystal substrate. The flask was heated at 120 °C under stirring for 12 h. Then the $Bi_2WO_6$ nanoparticles were grown on the $SiO_2$ photonic crystal substrate. After being washed with deionized water and ethanol and sintered at 400 °C for 1 h, the $Bi_2WO_6/SiO_2$ photonic crystal film was obtained. For comparison, the as-prepared $Bi_2WO_6/SiO_2$ photonic crystal film was immersed in 2 M NaOH to remove the $SiO_2$ photonic crystal and the ordinary $Bi_2WO_6$ film was obtained.

### 2.2. Characterization

The purity and the crystallinity of the as-prepared samples were characterized by powder X-ray diffraction (XRD) on a Japan Rigaku Rotaflex diffractometer using Cu Ka radiation while the voltage and electric current were held at 40 kV and 100 mA. The scanning electron microscope (SEM) characterizations were performed on a JEOL JSM-6700F field emission scanning electron microscope. The transmission electron microscope (TEM) analyses were performed by a JEOL JEM-2100F field emission electron microscope. The transmitted spectrum of the sample was measured by using a Hitachi U-3010 UV-Vis spectrophotometer.

### 2.3. Photocatalytic test

Photocatalytic activities of the $Bi_2WO_6$ films were evaluated by the degradation of RhB and phenol under visible light irradiation of a 500 W Xe lamp with a 400 nm cutoff filter. For the degradation of RhB and phenol, the reaction cell with a capacity of 100 mL was placed in a sealed black box of which the top was opened and the cutoff filter was placed to provide visible light irradiation. In each experiment, 10 pieces of $Bi_2WO_6$ films (2 cm × 2 cm) were placed on the bottom of the reaction cell with 50 mL of RhB solution ($1 \times 10^{-5}$ mol/L) or 50 mL of phenol solution (20 mg/L). The solution was not stirred during the reaction. Before illumination, the solution was equilibrated for about 120 min in the dark in order to reach adsorption–desorption equilibrium. At certain minute intervals, a 2 mL suspension was sampled. Then the adsorption UV–visible spectrum of the sampled solution was recorded using a Hitachi U-3010 UV-visible spectrophotometer.

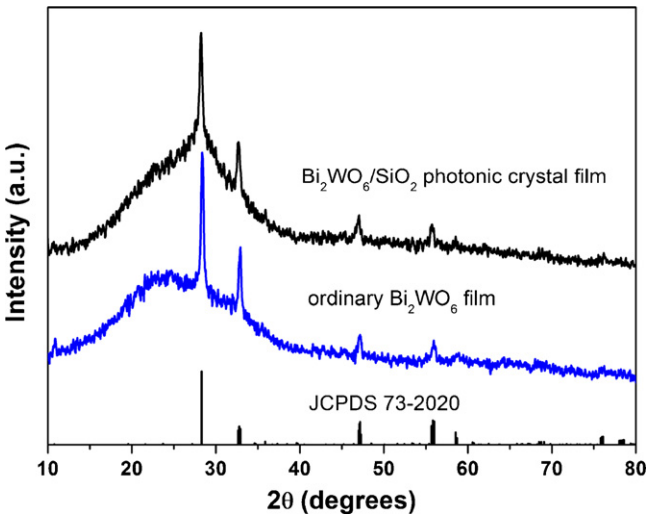


**Fig. 1.** XRD patterns of the as-prepared $Bi_2WO_6/SiO_2$ photonic crystal film and the ordinary $Bi_2WO_6$ film. The vertical lines at the bottom correspond to the standard XRD pattern of orthorhombic $Bi_2WO_6$ (JCPDS 73-2020).

## 3. Results and discussion

### 3.1. Characterizations of the $Bi_2WO_6/SiO_2$ photonic crystal sample

Fig. 1 shows the XRD patterns of the $Bi_2WO_6/SiO_2$ photonic crystal film and the ordinary $Bi_2WO_6$ film. For the $Bi_2WO_6/SiO_2$ photonic crystal film, it is found that the sample is well-crystallized in a single phase of $Bi_2WO_6$. All of the diffraction peaks can be well-indexed to JCPDS 73-2020 with a space group of B2ab (41). No other possible impurities can be detected. The XRD pattern of the ordinary $Bi_2WO_6$ film is similar to that of the $Bi_2WO_6/SiO_2$ photonic crystal film (Fig. 1). The morphology and microstructure of the $Bi_2WO_6/SiO_2$ photonic crystal film were studied by the microscope images. As shown from the SEM images in Fig. 2a, the $SiO_2$ photonic crystal film is composed of closely packed, hexagonal array of $SiO_2$ spheres with a diameter of 240 nm. Fig. 2b displays the SEM image of $Bi_2WO_6/SiO_2$ photonic crystal film, from which one can see the $Bi_2WO_6$ nanoparticles were uniformly deposited on $SiO_2$ spheres. The outlines of the sphere morphology are clear from Fig. 2b. The $Bi_2WO_6$ particles deposited on the $SiO_2$ sphere were nanoparticles with a size of about 20–100 nm from the SEM image of the $Bi_2WO_6/SiO_2$ photonic crystal film. Further close observation of the structure and morphology of the $Bi_2WO_6/SiO_2$ photonic crystal film were obtained from TEM images. The typical TEM image of some pieces of $Bi_2WO_6/SiO_2$ photonic crystal film mechanically exfoliated from the glass substrate is shown in Fig. 2c. From the TEM image, the $SiO_2$ spheres were closely packed and covered with smaller $Bi_2WO_6$ nanoparticles. It is also clear that the $Bi_2WO_6$ nanoparticles were tightly attached on the surface of the $SiO_2$ spheres with the size of about 20–100 nm, which is consistent with the results from the SEM images. The selective area electron diffraction (SAED) pattern recorded at the marked area of Fig. 2c is shown in Fig. 2d, which revealed the polycrystallinity of the deposited nanoparticles.

The light absorption property is an important factor to influence the photocatalytic efficiency. The light absorption of the $SiO_2$ photonic crystal film and the $Bi_2WO_6$ films were measured by detecting the transmission of these films under UV–vis light irradiation. Fig. 3 shows the transmission spectra of the films measured at normal incidence. An apparent transmission dip around 510 nm with a width of 100 nm can be observed for the $SiO_2$ photonic crystal film, which corresponds to the coherent Bragg scattering on a parallel set

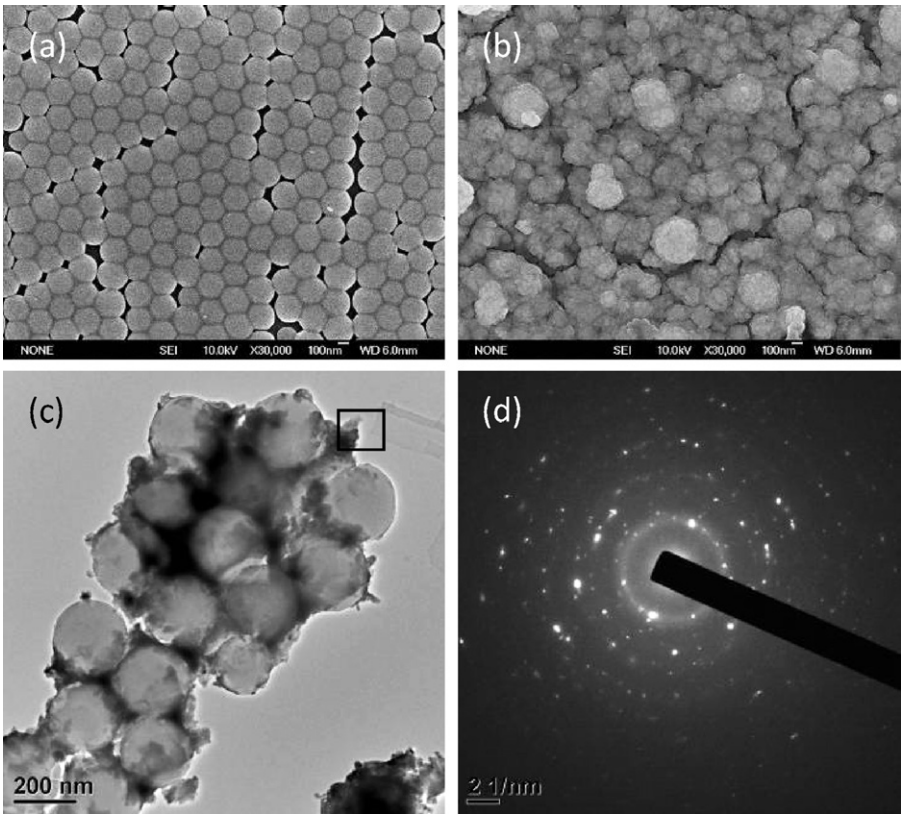


**Fig. 2.** (a) SEM image of the $SiO_2$ photonic crystal film. (b) SEM image of the $Bi_2WO_6/SiO_2$ photonic crystal film. (c) TEM image of the $Bi_2WO_6/SiO_2$ photonic crystal film. (d) SAED pattern recorded at the marked area of (c).

of (1 1 1) planes of the crystals. According to Bragg law for normal incidence, the position of the transmission dip ($\lambda_c$) can be expressed as:

$$\lambda_c = 2d_{(1\ 1\ 1)}(fnSiO_2 + (1-f)n_{air}) \quad (1)$$

where $f$ is the filling fraction of the $SiO_2$ phase, $n_{SiO_2}$ ($\approx$1.45) and $n_{air}$ (=1.0) are the refractive index of $SiO_2$ and air respectively. For fcc structures, $f$ = 0.74 and $d_{(1\,1\,1)}$ is associated with the pore size by Eq. (2):

$$d_{(1\ 1\ 1)} = \sqrt{2/3}D \quad (2)$$

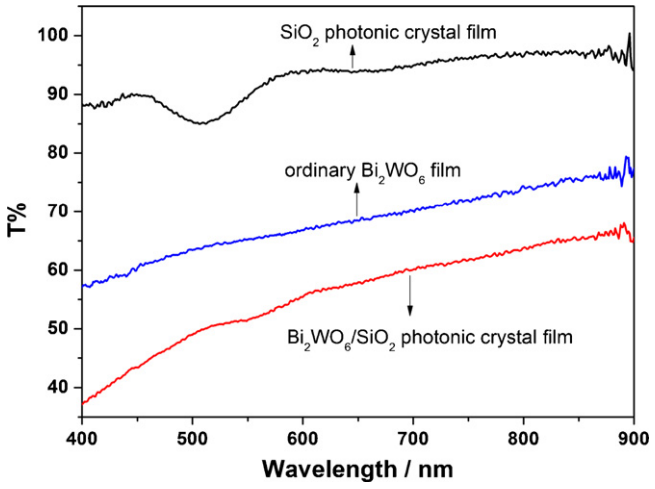


**Fig. 3.** Transmission spectra of the $SiO_2$ photonic crystal film, $Bi_2WO_6/SiO_2$ photonic crystal film and ordinary $Bi_2WO_6$ film measured at normal incidence.

where $D$ is the distance between neighboring spheres [28]. From the SEM image (Fig. 2a) of the $SiO_2$ photonic crystal film, the size of the silica spheres is about 240 nm. Then the $\lambda_c$ of the $SiO_2$ photonic crystal film for normal incidence is equal to 520 nm from Eq. (1), which is very close to its experimental data obtained from the transmission spectrum (Fig. 3). When the $Bi_2WO_6$ nanoparticles deposited on the $SiO_2$ photonic crystal film, the light transmission of the as-prepared $Bi_2WO_6/SiO_2$ photonic crystal film was dramatically decreased compared with the $SiO_2$ photonic crystal film, as shown in Fig. 3. The transmission dip of the $Bi_2WO_6/SiO_2$ photonic crystal film has a red shift to the wavelength around 550 nm because of the larger distance between neighboring $SiO_2/Bi_2WO_6$ spheres and the change of the refractive index compared with the bare $SiO_2$ photonic crystal film. The shallower transmission dip of the $Bi_2WO_6/SiO_2$ photonic crystal film may be due to the disorder from the deposited $Bi_2WO_6$ nanoparticles [29]. Different from the $Bi_2WO_6/SiO_2$ photonic crystal film, there is no transmission dip in the ordinary $Bi_2WO_6$ film (Fig. 3).

### 3.2. Photocatalytic performance

In order to evaluate the photocatalytic performance of the $Bi_2WO_6/SiO_2$ photonic crystal film visually, RhB was chosen as a representative model pollutant with rose color in appearance and a major absorption band at 553 nm. When the $Bi_2WO_6/SiO_2$ photonic crystal films in RhB solution were irradiated under visible light, the color of the RhB solution became shallow gradually with the decrease in its light absorption at 553 nm. Fig. 4a displays the temporal evolution of the spectral changes during the photodegradation of RhB over the $Bi_2WO_6/SiO_2$ photonic crystal film. A rapid decrease of RhB absorption at the wavelength of 553 nm is observed, along with an absorption band shift to shorter wavelengths. The absorption band shift is caused by N-demethylation of

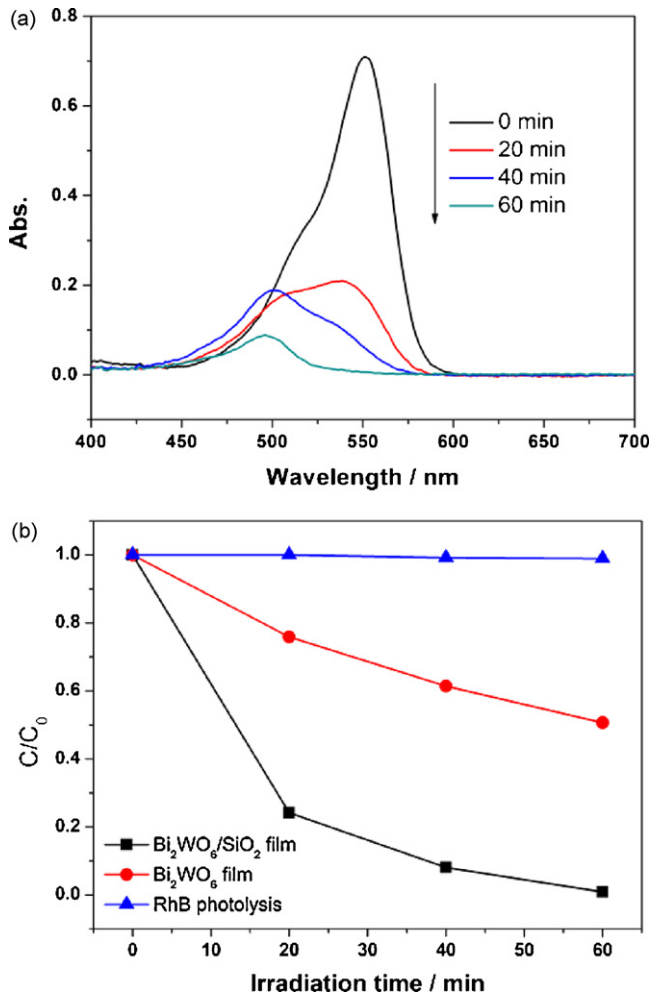


**Fig. 4.** (a) UV–visible absorption spectra of RhB during photodegradation in the presence of $Bi_2WO_6/SiO_2$ photonic crystal film. (b) Time profiles of $C/C_0$ of RhB during photodegradation by different photocatalysts.

RhB during photodegradation [30]. The sharp decrease and shift of the major absorption band within 20 min indicated that the as-prepared $Bi_2WO_6/SiO_2$ photonic crystal film has high photocatalytic activity on the degradation of RhB. The photodegradation efficiencies of RhB mediated by ordinary $Bi_2WO_6$ film as well as without photocatalyst (RhB photolysis) under visible-light illumination with otherwise identical conditions are displayed in Fig. 4b. It demonstrates that the photolysis of RhB is extremely slow without the photocatalyst under visible light illumination. However, 99% of the RhB was decolorized after 60 min if $Bi_2WO_6/SiO_2$ photonic crystal film is used as the photocatalyst, showing a high photocatalytic activity under visible light irradiation. For comparison, the photocatalytic property of ordinary $Bi_2WO_6$ film was tested. After being irradiated by visible light for 60 min, the degraded RhB was about 49%, indicating a much lower photocatalytic activity than that of the $Bi_2WO_6/SiO_2$ photonic crystal film.

As mentioned in Section 2, the ordinary $Bi_2WO_6$ film was prepared by removing the $SiO_2$ layer from the $Bi_2WO_6/SiO_2$ photonic crystal film. The crystallinity of these two $Bi_2WO_6$ films was similar from the XRD pattern. Then the different photocatalytic performance between the ordinary $Bi_2WO_6$ film and the $Bi_2WO_6/SiO_2$ photonic crystal film may be ascribed to their different film structures. Fig. 5 shows the SEM images of the ordinary $Bi_2WO_6$ film. The low magnified SEM in Fig. 5a exhibits a much flat surface compared with the $Bi_2WO_6/SiO_2$ photonic crystal film under the same magnification. This is because of the removal of the $SiO_2$ photonic crystal layer. From the high magnified SEM image, it could be observed the $Bi_2WO_6$ nanoparticles with the size of about 20–100 nm were evenly adhered to the surface of the glass substrate. It is obvious the morphology and particle size of the $Bi_2WO_6$ nanoparticles in the ordinary $Bi_2WO_6$ film are similar to that in the $Bi_2WO_6/SiO_2$ photonic crystal film from the SEM image, which confirms the discrepancy of the photocatalytic performance between the ordinary $Bi_2WO_6$ film and the $Bi_2WO_6/SiO_2$ photonic crystal film were mainly due to the difference of their film structures. As is well known, the photocatalytic performance is closely related to the contact surface area between the pollutant molecules and the photocatalytic materials. The surface area of the $Bi_2WO_6/SiO_2$ photonic crystal film is larger than that of the ordinary $Bi_2WO_6$ film due to their different film structures. This endows the $Bi_2WO_6/SiO_2$ photonic crystal film a higher photocatalytic activity. Another reason for the different photocatalytic performance may be ascribed to the different light absorption property which is also originated from their different film structures. As shown in Fig. 3, the $Bi_2WO_6/SiO_2$ photonic crystal film exhibits an enhanced visible light absorption around 550 nm (as shown in Fig. 3) which is very close to the major absorption band of RhB. It has been proved in the previous studies that the photodegradation of RhB by $Bi_2WO_6$ was partially attributed to a photosensitized mechanism [31]. When the visible light in the range of the absorption band of RhB was absorbed, photogenerated electrons in RhB transferred to the excited state of the dye and immediately injected to the conduction band of the $Bi_2WO_6$. This could finally lead to the degradation of RhB. The enhanced visible light utilization of the $Bi_2WO_6/SiO_2$ photonic crystal film could intensify the photosensitization of the adsorbed RhB and also lead to an improved photocatalytic performance.

Considering that the photodegradation of RhB is partially ascribed to a photosensitization process, the photocatalytic performance of the $Bi_2WO_6/SiO_2$ photonic crystal film was further evaluated by photodegradation of colorless phenol which is quite

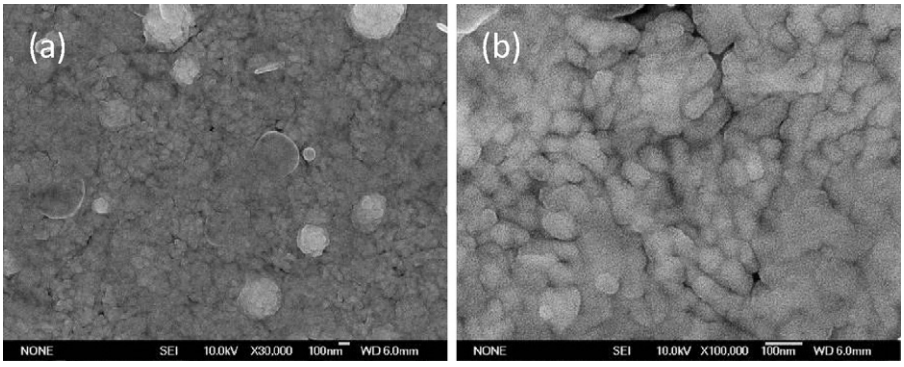


**Fig. 5.** (a) Low-magnification and (b) high-magnification SEM images of the ordinary $Bi_2WO_6$ film.

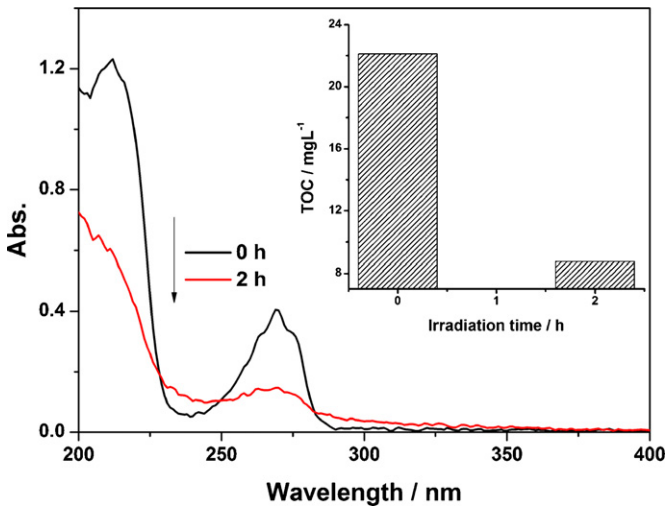


**Fig. 6.** UV absorption spectra of phenol during photodegradation in the presence of $Bi_2WO_6/SiO_2$ photonic crystal film under visible light irradiation (inset: variation of TOC of phenol aqueous solutions with irradiation time).

toxic but widely used and slowly degradable in the environment. Fig. 6 displays the temporal evolution of the spectral changes during the photodegradation of phenol over the $Bi_2WO_6/SiO_2$ photonic crystal film. A rapid decrease of phenol absorption at a wavelength of 269 nm was observed. The sharp decrease of the major absorption band indicates the as-prepared $Bi_2WO_6/SiO_2$ photonic crystal film exhibits excellent photocatalytic degradation of phenol. The degraded phenol was about 64% along with a total organic carbon (TOC) removal of about 60% within 2 h, which further confirm its excellent visible light driven photocatalytic performance.

## 4. Conclusion

$Bi_2WO_6/SiO_2$ photonic crystal films have been successfully synthesized by a direct chemical deposition method. The $Bi_2WO_6$ nanoparticles were uniformly deposited on the $SiO_2$ photonic crystal substrate from the SEM images. The as-prepared $Bi_2WO_6/SiO_2$ photonic crystal films exhibited excellent photocatalytic decomposition of RhB and phenol under visible light irradiation. Comparative studies indicated that the photocatalytic performance of the $Bi_2WO_6/SiO_2$ photonic crystal film was more efficient than that of ordinary $Bi_2WO_6$ film. The much better photocatalytic performance of the $Bi_2WO_6/SiO_2$ photonic crystal film was mainly ascribed to its special film structure.

## Acknowledgments

This work is financially supported by the National Natural Science Foundation of China (51102262, 50972155), National Basic Research Program of China (2010CB933503) and the Innovation Research of the Shanghai Institute of Ceramics (Y11ZCE1E0G).

## References

[1] H. Bai, Z. Liu, D.D. Sun, Chem. Commun. 46 (2010) 6542–6544.
[2] S. Ahmed, M.G. Rasul, R. Brown, M.A. Hashib, J. Environ. Manage. 92 (2011) 311–330.
[3] P. Fu, P. Zhang, Appl. Catal. B: Environ. 96 (2010) 176–184.
[4] J.G. Yu, H.G. Yu, B. Cheng, X.J. Zhao, J.C. Yu, W.K. Ho, J. Phys. Chem. B 107 (2003) 13871–13879.
[5] H. Lachheb, E. Puzenat, A. Houas, M. Ksibi, E. Elaloui, C. Guillard, J.M. Herrmann, Appl. Catal. B: Environ. 39 (2002) 75–90.
[6] Y. Ohko, I. Ando, C. Niwa, T. Tatsuma, T. Yamamura, T. Nakashima, Y. Kubota, A. Fujishima, Environ. Sci. Technol. 35 (2001) 2365–2368.
[7] J. Wu, F. Duan, Y. Zheng, Y. Xie, J. Phys. Chem. C 111 (2007) 12866–12871.
[8] S. Sun, W. Wang, J. Xu, L. Wang, Z. Zhang, Appl. Catal. B: Environ. 106 (2011) 559–564.
[9] L. Zhang, H. Wang, Z. Chen, P.K. Wong, J. Liu, Appl. Catal. B: Environ. 106 (2011) 1–13.
[10] H. Fu, S. Zhang, T. Xu, Y. Zhu, J. Chen, Environ. Sci. Technol. 42 (2008) 2085–2091.
[11] J.G. Yu, J.F. Xiong, B. Cheng, Y. Yu, J.B. Wang, J. Solid State Chem. 178 (2005) 1968–1972.
[12] J.W. Tang, Z.G. Zou, J.H. Ye, Catal. Lett. 92 (2004) 53–56.
[13] C. Wang, H. Zhang, F. Li, L. Zhu, Environ. Sci. Technol. 44 (2010) 6843–6848.
[14] L. Jiang, L. Wang, J. Zhang, Chem. Commun. 46 (2010) 8067–8069.
[15] L. Ge, J. Liu, Appl. Catal. B: Environ. 105 (2011) 289–297.
[16] C. Zhang, Y.F. Zhu, Chem. Mater. 17 (2005) 3537–3545.
[17] Z. He, C. Sun, S. Yang, Y. Ding, H. He, Z. Wang, J. Hazard. Mater. 162 (2009) 1477–1486.
[18] Y. Li, J. Liu, X. Huang, J. Yu, Dalton Trans. 39 (2010) 3420–3425.
[19] A. Kudo, S. Hijii, Chem. Lett. 28 (1999) 1103–1104.
[20] L.W. Zhang, Y.J. Wang, H.Y. Cheng, W.Q. Yao, Y.F. Zhu, Adv. Mater. 21 (2009) 1286–1290.
[21] J. Li, X. Zhang, Z. Ai, F. Jia, L. Zhang, J. Lin, J. Phys. Chem. C 111 (2007) 6832–6836.
[22] X. Zhao, T. Xu, W. Yao, C. Zhang, Y. Zhu, Appl. Catal. B: Environ. 72 (2007) 92–97.
[23] X. Zhao, Y. Wu, W. Yao, Y. Zhu, Thin Solid Films 515 (2007) 4753–4757.
[24] J. Xu, W. Wang, M. Shang, S. Sun, J. Ren, L. Zhang, Appl. Catal. B: Environ. 93 (2010) 227–232.
[25] S. Zhang, J. Shen, H. Fu, W. Dong, Z. Zheng, L. Shi, J. Solid State Chem. 180 (2007) 1456–1463.
[26] L. Zhang, C. Baumanis, L. Robben, T. Kandiel, D. Bahnemann, Small 7 (2011) 2714–2720.
[27] J.D. Joannopoulos, S.G. Johnson, J.N. Winn, R.D. Meade, Photonic Crystals, Molding the Flow of Light, 2nd edn., Princeton University Press, Princeton, 2008.
[28] S.L. Kuai, X.F. Hu, V.V. Truong, J. Cryst. Growth 259 (2003) 404–410.
[29] S.L. Kuai, Y.Z. Zhang, V.V. Truong, X.F. Hu, Appl. Phys. A 74 (2002) 89–90.
[30] C. Chen, W. Zhao, P. Lei, J. Zhao, N. Serpone, Chem. Eur. J. 10 (2004) 1956–1965.
[31] H. Fu, C. Pan, W. Yao, Y. Zhu, J. Phys. Chem. B 109 (2005) 22432–22439.